Macromolecular Bioscience
www.mbs-journal.de

Autoinducer Sensing Microarrays by Reporter Bacteria Encapsulated in Hybrid Supramolecular-Polysaccharide Hydrogels

Ping Li, Xiaoqiu Dou, Mareike Müller, Chuanliang Feng, Matthew Wook Chang, Martin Frettlöh, and Holger Schönherr**

A generally applicable strategy to obtain mechanically robust hydrogels for the incorporation and containment of functional reporter bacteria for the microarray and microparticle-based detection and signaling of *N*-acyl homoserine lactone autoinducers ($3OC_{12}HSL$) at relevant concentrations is reported. For reinforcing hydrogels of 1,4-bi(phenylalanine-diglycol)-benzene (PDB), a hybrid hydrogel is formed by the combination of PDB self-assembly with Ca^{2+} mediated alginate crosslinking. The different assembly mechanisms are shown not to interfere with each other and despite the more than four-fold increased moduli of the hydrogels, diffusion of autoinducers into the gels remains efficient and *Escherichia coli* pLuxR-green fluorescent protein (GFP) reporter bacteria are proliferating. Templating affords reporter bacteria-loaded hydrogels with controllable shape and size. Upon exposure to $3OC_{12}HSL$, the embedded bacteria exhibit an up to 12 ± 3 times increase in fluorescence intensity due to autoinducer-triggered GFP expression. This approach can serve as a potentially generally applicable strategy to sensitively detect bacteria via their secreted autoinducers.

1. Introduction

The detection of bacteria and bacterial infections is an area of intensive research activities, not only in recent years. Among the various new formats for rapid, sensitive and selective bacteria detection, vesicle based approaches,[1,2] autonomously reporting hydrogel films,[3] as well as hydrogel dot microarrays[4] have garnered particular attention. These formats mainly rely on the detection and reporting of secreted bacterial enzymes,[5] DNA,[6] and virulence factors.[7] For many infections, such as wound infections, bacteria reside in a so-called biofilm, which represents a confluent community of bacteria protected by an extracellular polymeric matrix.[8] It is generally accepted that microbial biofilms possess implications in wound infections, increased antibiotic resistance, and hard-to-heal wounds.[9] Thus the detection of infection with a colorimetric signaling only after reaching the so-called critical colonization threshold or the early identification of biofilm formation is of prime importance for permitting early and effective intervention.[10] To adequately address these challenges, one promising avenue is the detection of small molecules involved in biofilm formation, the so-called autoinducers. Microbial cells rely on the production, secretion, and detection of autoinducers to regulate gene expression in response to bacteria population density fluctuations (quorum sensing).[11,12] When a critical population density is reached or the autoinducer concentration is above a certain threshold, the autoinducers can be detected by the bacteria. At high bacterial density particular gene expression programs are triggered, such as biofilm formation.[13] Certain strains of bacteria possess specific autoinducers for quorum sensing: Gram-negative bacteria mainly use *N*-acyl homoserine lactones (AHLs), while Gram-positive bacteria mainly adapt oligopeptides for this population-dependent communication, among others.[14,15]

To utilize the quorum sensing mechanism for biofilm detection, microorganisms have been genetically modified to produce reporter proteins in a dose-dependent manner in the presence of target autoinducers.[16]

For application as whole-cell sensors, these genetically modified microorganisms must be safely entrapped in a matrix. Among the various materials reported, hydrogels consisting of crosslinked hydrophilic networks have been widely used

P. Li, Dr. X. Q. Dou, Dr. M. Müller, Prof. H. Schönherr
Physical Chemistry I and Research Center of Micro and Nanochemistry and Engineering (Cμ)
Department of Chemistry and Biology
University of Siegen
Adolf-Reichwein-Str. 2, 57076 Siegen, Germany
E-mail: m.mueller@chemie-bio.uni-siegen.de; schoenherr@chemie.uni-siegen.de

Prof. C. L. Feng
State Key Lab of Metal Matrix Composites
School of Materials Science and Engineering
Shanghai Jiaotong University
800 Dongchuan Road, 200240 Shanghai, P. R. China

Prof. M. W. Chang
Department of Biochemistry
Yong Loo Lin School of Medicine
National University of Singapore
14 Medical Drive, Singapore 117599, Singapore

Prof. M. W. Chang
NUS Synthetic Biology for Clinical and Technological Innovation (SynCTI)
Life Sciences Institute
National University of Singapore
28 Medical Drive, Singapore 117456, Singapore

Dr. M. Frettlöh
Quh-Lab Food Safety
Siegener Str. 29, 57080 Siegen, Germany

The ORCID identification number(s) for the author(s) of this article can be found under https://doi.org/10.1002/mabi.201700176.

DOI: 10.1002/mabi.201700176

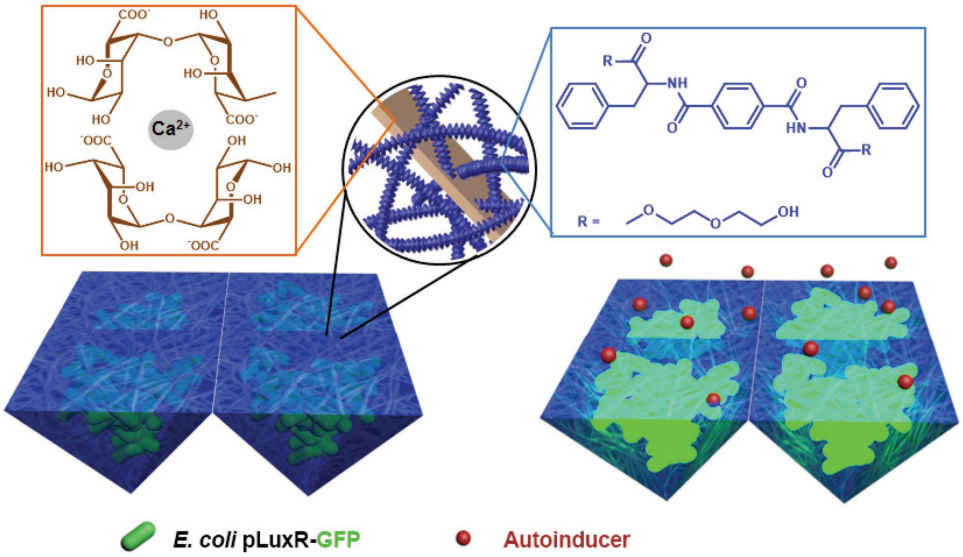

Figure 1. Scheme of micropatterned PDB-alg-Ca hydrogel and corresponding molecular structures. The *E. coli* pLuxR-GFP reporter bacteria express GFP upon recognition of the autoinducer (here: *N*-dodecanoyl-L-homoserine lactone). Left: Micropatterned PDB-alg-Ca hydrogels with embedded bacteria; top: schematic of nanofibrillar assemblies formed by the PDB gelator that self-assembles into nanofibers in the presence of cross-linked alginate-Ca; right: autoinducer-induced GFP expression of reporter bacteria *E. coli* pLuxR-GFP safely entrapped in the patterned PDB-alg-Ca hydrogel.

for cell encapsulation owing to their cytocompatibility, degradability, and mass transfer efficiency.[17,18] The gels, inside which cells can proliferate and function, protect the cells from detrimental environmental conditions (e.g., pH, heat, and toxic compounds). Hydrogels also facilitate the isolation of cells from the surrounding media for convenient handling. The ideal hydrogel matrix for microorganism immobilization would be (1) biocompatible; (2) permeable to nutrients, to oxygen, to incoming signaling molecules and to the outgoing response;[19] (3) mechanically and chemically stable to protect bacteria,[20] etc.

Given the different environments in which the biosensors may be used, hydrogels fabricated from polymers, such as poly(ethylene oxide),[21] poly(vinyl alcohol), alginate,[22] gelatin,[23] have been used as entrapping matrices.[24,25] As an alternative, supramolecular hydrogels formed via noncovalent interactions among small molecules have been used in biomedical science in behalf of high water content,[26] stimuli response performance,[27,28] and favorable biocompatibility, e.g., the mild self-assembly process without the introduction of potential harmful agents.[29] The controllable physical and biochemical properties from rational molecular design are used to tune the behavior and functionality of the enclosed cells.[30]

While we showed the feasibility of supramolecular hydrogels formed by low molar mass gelator self-assembly for reporter bacteria encapsulation in a microarray format with single bacteria per well for *N*-acyl homoserine lactone autoinducer-reporting *Escherichia coli* pTetR-LasR-pLuxR-green fluorescent protein (GFP) (*E. coli* pLuxR-GFP),[31,32] the utilized supramolecular hydrogels possessed poor mechanical properties.

As a promising strategy for reinforcement, the formation of interpenetrating networks (IPNs) of supramolecular hydrogels and the biopolymer alginate has been reported by some of us.[33] However, instead of utilizing a thermal trigger as has been reported before,[33] a solvent shift method was used to trigger the self-assembly of the 1,4-bi(phenylalanine-diglycol)-benzene (PDB) gelator through noncovalent interactions.[34] The gel formed allows calcium ions to penetrate and to cross-link the incorporated linear polysaccharide alginate.[35,36] We applied this new strategy, as reported here, as an element of a generally applicable approach to obtain mechanically robust hydrogels for the incorporation and containment of functional reporter bacteria for the microarray and microparticle-based detection and signaling of *N*-acyl homoserine lactone autoinducers ($3OC_{12}HSL$) at relevant concentrations secreted by *Pseudomonas aeruginosa* (*P. aeruginosa*) (**Figure 1**). In addition to the fabrication of gelator-polysaccharide hybrid hydrogels and their detailed characterization, the central aim of this study was to investigate bacteria viability and autoinducer diffusion and to demonstrate signaling and microarray based sensing inside the hybrid hydrogels and the analysis of the autoinducer-triggered expression of GFP by *E. coli* pLuxR-GFP.

2. Experimental Section

2.1. Materials

All the chemicals were purchased from Sigma-Aldrich and were used without further purification unless otherwise noted. Poly(ethylene glycol) diacrylate (PEGDA, M_n = 250 g mol^{-1}, Sigma-Aldrich) was purified using aluminum oxide 90 active neutral (0.063–0.200 mm, Merck KGaA). Luria–Bertani medium (LB broth), and LB agar were purchased from Carl Roth. Milli-Q water from a Millipore Direct Q8 system (Millipore Advantage A10 system, Schwalbach, with Millimark Express 40 filter, Merck,

Germany) with a resistivity 18.2 MΩ cm was used in all experiments and to prepare all buffers.

2.2. Gelator Synthesis

The gelator PDB was synthesized with 59% yield in a three-step conventional liquid phase reaction according to refs. [33,38] (see also Scheme S1 in the Supporting Information).

2.3. Hydrogel Preparation

PDB was dissolved in dimethyl sulfoxide (DMSO) to form a solution with concentrations of 100 and 150 mg mL^{-1}, respectively. Sodium alginate was dissolved into Milli-Q water to form an alginate solution with concentrations of 5, 7, 10, and 20 mg mL^{-1}, respectively.

For preparing 3 mg mL^{-1} (or 2 mg mL^{-1}) PDB hydrogels: 490 µL of Milli-Q water was mixed with 10 µL of 150 mg mL^{-1} (or 100 mg mL^{-1}) PDB solution under continuous vortexing (RS-VA10, Phoenix Instrument, Germany) for 30 s, followed by 5 min still standing. The hydrogels were directly used for scanning electron microscopy sample preparation. For atomic force microscopy and transmission electron microscopy samples preparation the hydrogels were diluted with 4.5 mL Milli-Q water.

For preparing PDB-alg-Ca hydrogels with 3 mg mL^{-1} (or 2 mg mL^{-1}) PDB and 5 mg mL^{-1} alginate: 490 µL of 5 mg mL^{-1} alginate solution was mixed with 10 µL of 150 mg mL^{-1} (or 100 mg mL^{-1}) PDB solution under continuous vortexing for 30 s, followed by 5 min still standing. 5 µL of 100×10^{-3} M $CaCl_2$ solution was added onto the gel, and the formed gel was termed PDB-alg-Ca hydrogel. The formed gels were used for scanning electron microscopy samples preparation.

2.4. Fourier Transform Infrared (FT-IR) Spectroscopy

Transmission FT-IR spectra of dried gels were taken using a Bruker EQUINOX55 Instrument. The KBr disk technique was used for the solid-state measurement. The samples were scanned between wavenumbers of 4000–400 cm^{-1}.

2.5. X-Ray Photoelectron Spectroscopy (XPS)

PDB, PDB-alginate, and PDB-alg-Ca hydrogels were dried on silicon substrates. X-ray photoelectron spectroscopy was carried out using the Kratos AXIS ULTRA DLD instrument with Al (Mono) anode in 1000.0 meV step. The data was processed using CasaXPS software.

2.6. Circular Dichroism (CD) Spectroscopy

CD spectra were recorded using a Chirascan CD-spectrometer (Applied Photophysics, UK). A Quartz cuvette (Hellma Analytics, Germany) with 0.1 mm path length was used for gel measurements and a quartz cuvette (Hellma Analytics, Germany) with 1 mm path length was used for gelator solution measurements.

2.7. Transmission Electron Microscopy (TEM)

TEM images were obtained with an analytical transmission electron microscope (JEM-2010). The samples were prepared by placing drops of the diluted aqueous gel suspension onto TEM copper grids, which were dried under ambient conditions.

2.8. Scanning Electron Microscopy (SEM)

Hydrogels were immersed into liquid nitrogen for 15 min and then transferred to the lyophilizer (FD-1, ZiBo SenYuan Electric Co., China) until all the frozen water sublimated. The morphologies of the PDB and PDB-alg-Ca dried gels from freeze drying were imaged using a FEI QUANTA 250 (USA). Samples were coated with 8–10 nm gold via a sputtering coater (S 150B, Edwards, UK).

2.9. Atomic Force Microscopy (AFM)

PDB and PDB-alg hydrogels suspensions were rapidly pipetted onto freshly cleaved mica surfaces, which were dried under ambient conditions. AFM measurements were carried out using a multimode NanoNavi E-sweep AFM (SII Nanotechnology, Japan) in tapping mode. A silicon tip/cantilever (NSC11/AlBS, Mikro Masch) was used with a resonance of 60 kHz and a nominal force constant of 3.0 N m^{-1}. All measurements were performed under ambient conditions (atmospheric pressure, ≈30% relative humidity, 24 °C). AFM images were analyzed using an offline AFM software (BinOffline500-0609, SII Nanotechnology, Japan).

2.10. Rheological Measurements

The rheological properties of the PDB and PDB-alg-Ca hydrogels were measured using a Rotary Rheometer (Gemini HR nano, Malvern, UK) with a 20 mm diameter plate-plate geometry (steel). Dynamic strain scans were performed at 1 Hz frequency to determine the linear viscoelastic region at 25 °C. Dynamic frequency sweep tests were performed in which a sinusoidal shear strain of constant peak amplitude (1%) was applied over 0.01–10 Hz frequencies at 25 °C.

2.11. Hydrogel Permeability Tests

The permeability of PDB and PDB-alg-Ca hydrogels for autoinducers was studied by measuring the diffusion of *N*-dodecanoyl-L-homoserine lactone-3-hydrazone-fluorescein (FITC-AHL, purchased from Biomol, Germany) into the gels over time. 980 µL Milli-Q water was mixed with 20 µL of 150 mg mL^{-1} PDB solution under continuous vortexing for 30 s, then 100 µL of the mixture was added to each well of a 96 well plate, followed by 5 min still standing. 980 µL of 5 mg mL^{-1} alginate

solution was mixed with 20 µL of 150 mg mL^{-1} PDB solution under continuous vortexing for 30 s, then 100 µL of the mixture was added to each well of a 96 well plate, followed by 5 min still standing. 3 µL of 100×10^{-3} M $CaCl_2$ solution was added upon the gel. After 30 min, 100 µL of 1×10^{-5} mol L^{-1} FITC-AHL solution on top of the gel for each well. After immersion for 1, 2, 3, 6, 15, 30, 60, or 120 min, 50 µL of the supernatant was withdrawn and pipetted into black flat-bottom 96 well plate (Greiner Bio-One, Germany). The fluorescence intensities of 1×10^{-5} mol L^{-1} FITC-AHL solution and withdrawn supernatant were measured using a microplate reader (Tecan SAFIRE, Tecan, Switzerland).

2.12. Fabrication of PEGDA Microwell Arrays

An AggreWell400Ex chip (STEMCELL Technologies, Canada) was used as a template to fabricate polydimethylsiloxane (PDMS) stamps. A mixture of silicon elastomer and curing agent (10:1) was degassed for 30 min and poured onto the AggreWell400Ex chip, followed by incubation at 70 °C for 1 h. The PDMS was peeled off and cut with scalpel to form PDMS molds. As shown in Scheme S2 (Supporting Information), PDMS molds were pressed on the polystyrene petri dish to form conformal contact. A drop of PEGDA precursor with 0.2 wt% 2-hydroxy-1-[4-(2-hydroxyethoxy)-phenyl]-2-methyl-1-propanone (Irgacure 2959) was placed at one end of the mold and the precursor filled the space between mold and substrate due to capillary forces. After 15 min of UV irradiation (CL-1000 series UV crosslinker, with CL-1000L Model 365 nm UV tubes, 5 × 8 W), the PDMS mold was peeled off, and the formed hydrogel was rinsed with excess ethanol and MilliQ-water.

2.13. Hydrogel Micropatterning

10 µL PDB in DMSO (150 mg mL^{-1}) was mixed with 490 µL alginate solution (5 mg mL^{-1}) under continuous vortexing (RS-VA10, Phoenix instrument, Germany); then a 100 µL drop of the gel mixture was pipetted onto PEGDA microwell arrays and was covered by a clean, sterilized PDMS, applying gentle pressure. After 5 min, the PDMS cover slide was gently removed and 10 µL $CaCl_2$ solution (100×10^{-3} M) was added on the top of gels.

2.14. Bacteria Culture

E. coli TOP10 pTetR-LasR-pLuxR-GFP[31] (*E. coli* pLuxR-GFP as abbreviation) was cultured according to published protocols.[32]

2.15. Characterization of *E. coli* pLuxR-GFP Embedded in the Microscale Hydrogels

The bacteria suspension at a certain density ($OD_{600} \approx 0.5$) was prepared as described above. The scheme of fabrication procedure is shown in Scheme S3 (Supporting Information). 10 µL PDB in DMSO (150 mg mL^{-1}) was mixed with 490 µL bacteria alginate-LB suspension (5 mg mL^{-1} alginate) to form bacteria encapsulated PDB-alg-Ca micropatterned hydrogels. 200 µL fresh LB media with or without $3OC_{12}HSL$ was applied to cover the microwells completely. The samples were observed under an inverted fluorescence microscope (Axiovert 135, Carl Zeiss, Germany) after 2–6 h incubation. Fluorescent images were quantitatively analyzed using ImageJ software. The fluorescent signal intensity was measured across ≥ 3 wells, allowing for the determination of average fluorescent intensity per well.

3. Results and Discussion

PDB gelators possess the ability to form hydrogels in aqueous medium by self-assembly through the combination of hydrogen bonds, hydrophobic, and π–π stacking interactions, which has been amply demonstrated in our previous studies.[33,34,37,38] However, the supramolecular hydrogels formed exhibit poor mechanical properties, which may lead to an instability of hydrogel objects under applied external mechanical forces, such as vortex or agitation. As shown in Figure S2 (Supporting Information), the applied mechanical forces caused a PDB hydrogel to collapse. In our former studies a strategy for reinforcement was presented.[33] Here the biopolymer alginate was additionally incorporated to form a two component interpenetrated network-type hydrogel with improved mechanical properties.[38] However, the gel-to-sol transition temperature of the PDB hydrogels was determined above 80°C, which is not suitable for the encapsulation of sensitive biological agents or cells.

Herein, the solvent shift method was adapted to trigger the self-assembly of PDB gelators, followed by reinforcement by crosslinking alginate additionally. The hydrogel preparation is schematically illustrated in **Figure 2**. A PDB solution in DMSO was mixed with an aqueous alginate solution. The PDB gelators self-assembled in presence of alginate into hydrogels that still allowed the diffusion of calcium ions into the gels to crosslink the incorporated alginate. The solvent-change triggered self-assembly of the low molar mass gelator PDB and the ionic crosslinked alginate gave rise to translucent stiff PDB-alg-Ca hydrogels (Figure S3, Supporting Information).

The chemical composition of the formed PDB-alg-Ca hydrogels was assessed by FT-IR spectroscopy, as shown in **Figure 3**a. The bands at 1640 and 1413 cm^{-1} are assigned to the antisymmetric and symmetric stretching vibrations of the carboxylate group of alginate,[39] while bands at 1736, 1650, and 1543 cm^{-1} are attributed to the C=O stretching vibration and the amide I and amide II bands of typical secondary amides of PDB molecule, respectively. The FT-IR spectrum of PDB-alginate and PDB-alg-Ca gels exhibited both the characteristic absorption bands of PDB and alginate, which suggests that a hybrid hydrogel was obtained that contains both PDB and alginate. The broad peaks at 3442 and 3296 cm^{-1} indicated the inter- and intramolecular hydrogen bonding.[38] The NH— signals were observed in the range of 3320–3270 cm^{-1}, whereas the signals originating from the CO— moieties fell between 1680 and 1630 cm^{-1}. Both ranges are characteristic for intermolecular hydrogen bonding between the amide groups.[38]

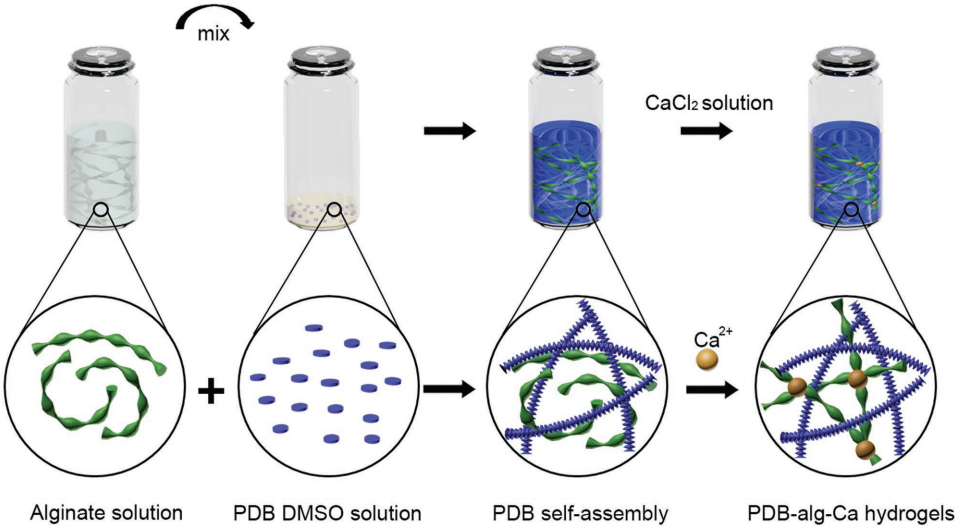

Figure 2. Schematic of the PDB-alg-Ca hydrogel preparation process: PDB DMSO solution was mixed with aqueous alginate solution, the solvent change triggered the self-assembly of PDB gelators with alginate dispersed inside the formed hydrogel; then a $CaCl_2$ solution was added to the hydrogel, leading to Ca^{2+} diffused into the hydrogel and the formation of alginate-based crosslinks.

The superstructure of the self-assembled gelators in PDB and PDB-alg-Ca hydrogels was assessed by CD measurements. The measured CD bands of PDB in H_2O solution (black dashed line in Figure 3b) showed λ_{max} values at 217 nm (peak) and 240 nm (trough), which are due to the amide carbonyl groups and phenyl group in the 1,4-benzenedicarboxamide, respectively.[40,41] Compared to the PDB solution, the PDB hydrogel showed spectral peaks that were shifted to 226 and 266 nm (black line in Figure 3b), indicating the self-assembly in the hydrogel.[34] The alginate solution and the alginate-Ca hydrogels showed no obvious CD peaks, suggesting no or only few ordered structures. The CD spectrum of PDB-alg-Ca hydrogels exhibited the characteristic peak positions of the PDB hydrogels, which indicates that the presence of alginate has no significant influence on the self-assembled structures of PDB gelators.

The elemental composition of formed hybrid gels was analyzed by an XPS. The XPS survey spectra of PDB, PDB-alginate, and PDB-alg-Ca gels shown in **Figure 4**a revealed the C 1s, O 1s, N 1s, Na 1s, Ca 2p, and Si 2p signals at 285, 532, 400, 1071, 348, and 102 eV, respectively. The observed Si signal originated from the silicon substrates used for gel supporting. As shown in **Table 1**, the elemental ratios for PDB gels (O/C 0.30 and N/C: 0.05) were close to theoretical value (O/C: 0.29 and N/C: 0.06) calculated by the chemical structure of PDB ($C_{34}H_{40}O_{10}N_2$). The incorporation of sodium alginate increased the oxygen content from ≈21.5 to ≈29.5 at%, while the concentration of Na increased to 1.9 at%. For PDB-alg-Ca gels, the content of Na decreased to almost zero and that of Ca increased to 1.0 at%. The guluronic acid units of alginate captured calcium ions to form calcium alginate network, when mixed with supernatant containing calcium ions.[42] Therefore, it is reasonable to observe that the PDB-alg-Ca hybrid gels contained Ca instead of Na.

The high resolution C 1s spectra of PDB and PDB-alg-Ca gels were fitted with four unique carbon peaks (Figure 4b,c): C—C/C—H (284.6 eV), C—O (286.0 eV), N—C=O (287.4 eV), and O—C=O (288.5 eV), respectively. For PDB gel, the ratio of

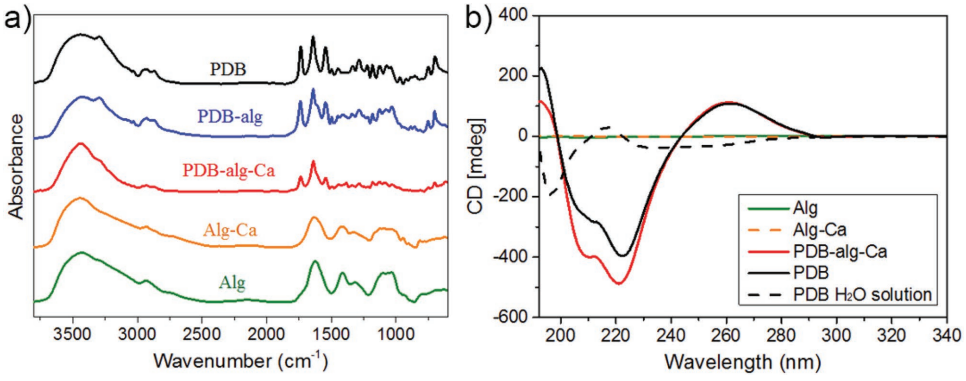

Figure 3. a) FT-IR spectra of PDB, PDB-alginate, PDB-alg-Ca, alginate-Ca and alginate dried gels; b) circular dichroism (CD) spectra of PDB, alginate-Ca, PDB-alg-Ca hydrogels (PDB: 3 mg mL^{-1}; alginate: 5 mg mL^{-1}), alginate solution (5 mg mL^{-1}), and PDB water solution (0.3 mg mL^{-1}).

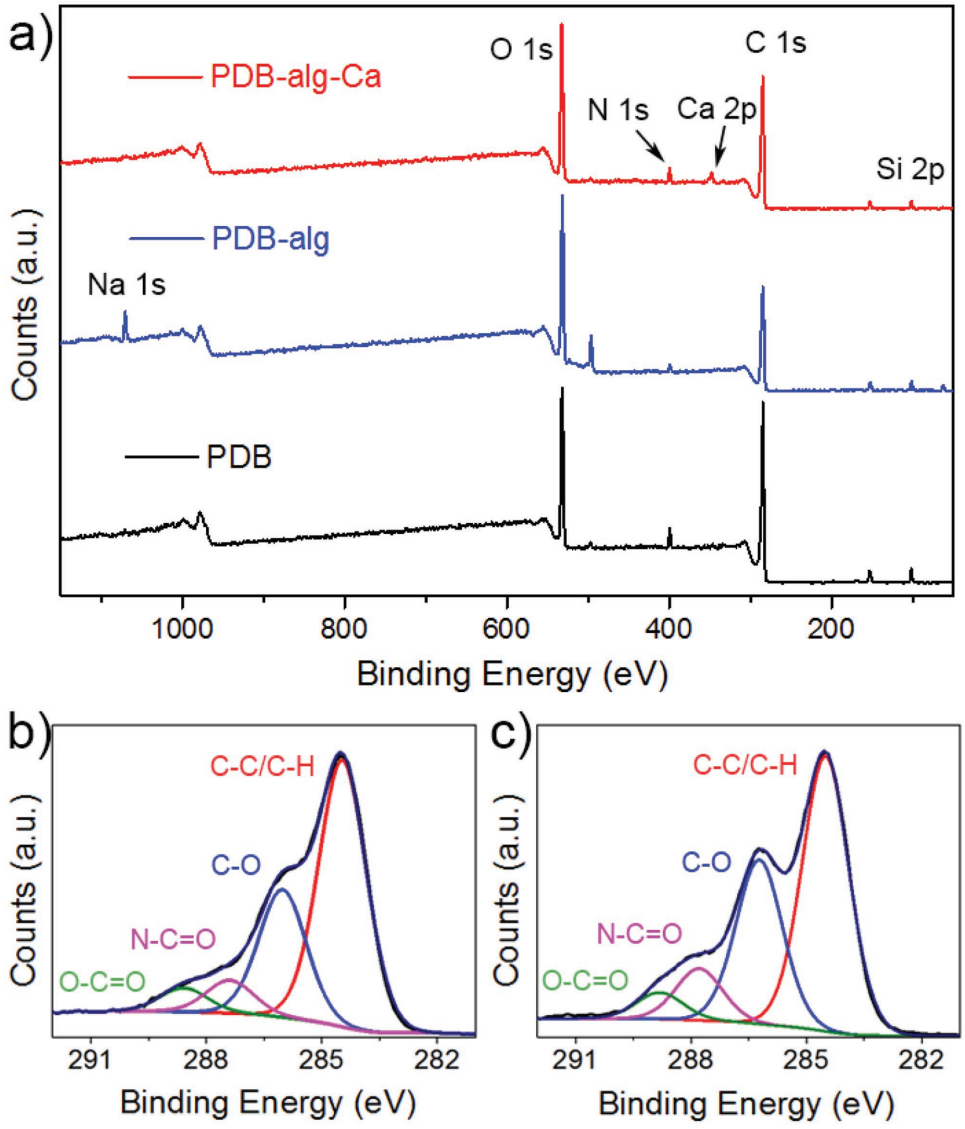

Figure 4. a) XPS survey spectra of PDB, PDB-alginate, and PDB-alg-Ca dried gels on Si substrates; C 1s high resolution spectra of b) PDB and c) PDB-alg-Ca dried gels, the peaks are assigned to the following C 1s signal: C—C/C—H (284.6 eV; red), C—O (286.0 eV; blue), N—C=O (287.4 eV; pink), O—C=O (288.5 eV, green).

C—C and C—O was 2:1, which is in agreement with the theoretical ratio (2:1) calculated on the basis of the stoichiometry. By contrast, for the PDB-alg-Ca gel, the ratio of C—C and C—O was found to be 5:3, the increase of the C—O contribution is attributed to the incorporation of alginate ($(C_6H_8O_6)_n$).

The 3D fibrous structures of PDB and PDB-alginate gels were visualized under SEM after freeze drying (**Figure 5**a,b). The 3D networks in PDB gels consist of twisted and entangled fibers with 430 ± 170 nm diameter and hundreds micrometers in length. For PDB-alginate gels, the fibers measured 550 ± 110 nm in diameter and hundreds micrometer in length. The distribution of fiber diameters was presented in Figure S5 (Supporting Information). Among the fibers, dispersed layer structures were noticed (Figure 5b). With increasing the

Table 1. Elemental composition in atom% as determined by XPS of PDB, PDB-alginate, and PDB-alg-Ca dried gels.

Sample	XPS atomic concentrations [at%]					
	C 1s 284.6 eV	O 1s 531.5 eV	N 1s 399.5 eV	Na 1s 1070.5 eV	Ca 2p 347.5 eV	Si 2p 101.5 eV
PDB	70.1	21.5	3.4	–	–	5.0
PDB-alginate	63.8	29.5	1.4	1.9	–	3.4
PDB-alg-Ca	66.6	26.2	2.8	–	1.0	3.4

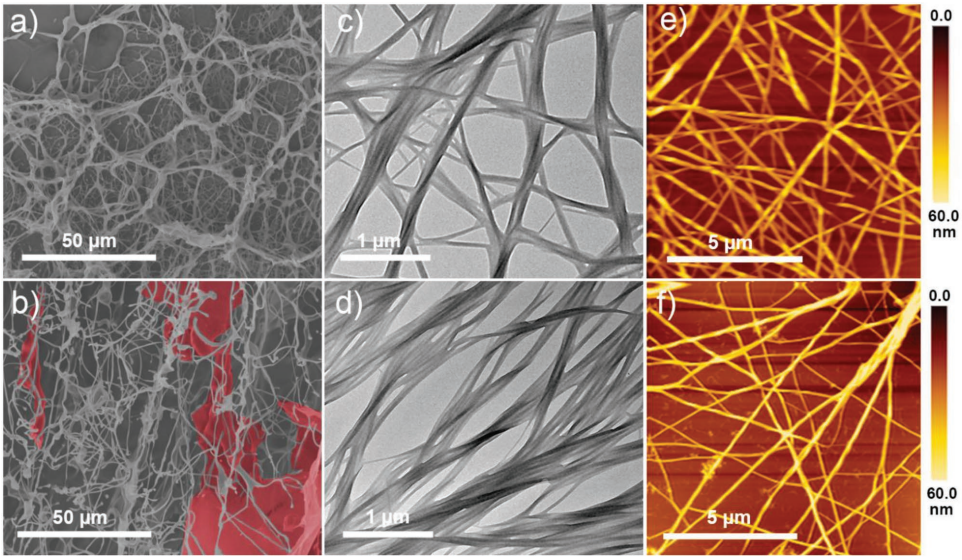

Figure 5. SEM images of freeze-dried a) PDB gel and b) PDB-alg-Ca gel, PDB: 2 mg mL^{-1}, alginate: 5 mg mL^{-1}, the layer structures were labeled by red color using Adobe Photoshop CS5.1; TEM images of fibrous structure of c) PDB gel and d) PDB-alginate gel, PDB: 0.2 mg mL^{-1}, alginate: 0.5 mg mL^{-1}; AFM images of e) PDB gel and f) PDB-alginate gel, PDB: 0.2 mg mL^{-1}, alginate: 0.5 mg mL^{-1}.

alginate concentration from 5 to 7 mg mL^{-1}, more of this layered morphology was observed (Figure S4a, Supporting Information). For the alginate-Ca gel, a continuous polymeric film was discerned without any visible fibers (Figure S4b, Supporting Information). Thus the appearance of these dispersed layers among the fibers is attributed to the incorporation of alginate. Both PDB and PDB-alg-Ca gels exhibited fibers with high aspect ratios, which indicates highly anisotropic intermolecular interactions between gelator molecules.[34]

Structures consisting of fibers and fiber bundles were also observed under TEM (Figure 5c,d). When the concentration of PDB was decreased from 2 to 0.2 mg mL^{-1} the fiber structures still could be observed, which indicates the PDB gelator could self-assemble at low concentration. The thin fibers have dimensions of 26 ± 7 nm in diameter, while bundles or entanglements of fibers were with 183 ± 29 nm in diameter, as measured from the TEM images. Compared to diluted PDB gels, PDB-alginate gels possess thin fibers with a diameter of 23 ± 6 nm and bundles with a diameter of 220 ± 84 nm, which may be due to the inhomogeneous distribution of fibers.

The morphologies of nanofibers formed in the network were also measured by AFM (Figure 5e,f). Both PDB gels and PDB-alg-Ca gels showed an interwoven network of numerous nanofibers with heterogeneous widths and large aspect ratios. No obvious layer structure was detected, which may be due to the low concentration of alginate (0.5 mg mL^{-1}). All the results of the morphology investigation indicate that the incorporation of alginate does not significantly affect the fibrous structure formed from the self-assembly of PDB.[34,38]

Dynamic oscillatory rheology experiments were performed to investigate the mechanical properties of PDB and PDB-alg-Ca hydrogels. Nondestructive frequency sweep tests were performed at 1% stain from 0.01 to 10 Hz, which is within the linear viscoelastic range determined by a shear strain amplitude sweep test.[43] From the frequency sweep tests shown in **Figure 6**, it is evident that PDB and PBD-alg-Ca

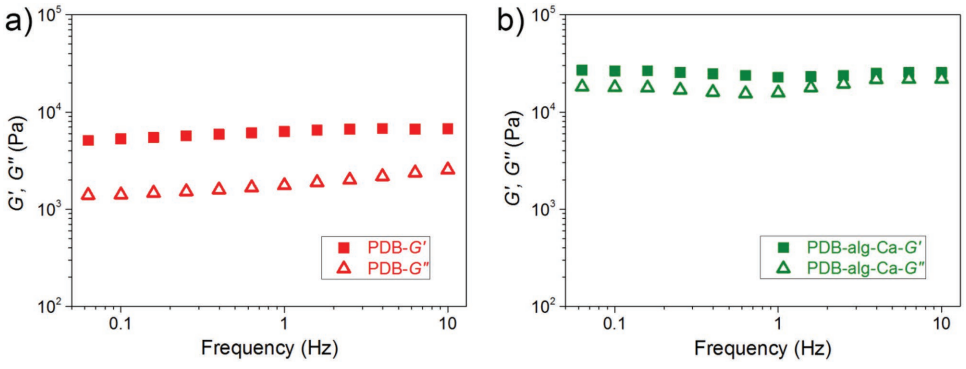

Figure 6. Frequency sweep test of a) PDB hydrogels (3 mg mL^{-1}), and b) PDB-alg-Ca hydrogels (3 mg mL^{-1} PDB and 5 mg mL^{-1} alginate) from 0.01 to 10 Hz, at 1% strain and 25 °C, elastic modulus G' (square solid symbol), viscous modulus G'' (triangle hollow symbol).

hydrogels exhibit typical solid-like rheological behavior with the elastic moduli (G', ≈5.7 × 10^3 Pa for PDB; ≈2.5 × 10^4 Pa for PBD-alg-Ca) dominating the viscous moduli (G'', ≈1.7 × 10^3 Pa for PBD; 1.8 × 10^4 Pa for PBD-alg-Ca) over the entire investigated frequency range. The G' values of PBD-alg-Ca hydrogels are around 4.4 times larger than those of PDB hydrogels. The formation of an interpenetrating network in these two component hybrid gels is thus an effective way to improve the viscoelastic properties of the hydrogels.

For the anticipated application, the diffusion of autoinducers to the encapsulated reporter bacteria is necessary. Hence the permeability of PDB and PDB-alg-Ca hydrogels toward $3OC_{12}HSL$ was assessed by immersing hydrogels into a solution of a fluorescently labeled autoinducer (FITC-AHL) and measuring the concentration of FITC-AHL inside hydrogels over time, as shown in **Figure 7**a. For both PDB and PDB-alg-Ca hydrogels, the FITC-AHL concentration in the hydrogel increased rapidly in the first 10 min and reached the equilibrium in around 30 min. The FITC-AHL uptake was fast in the initial contact period and the gradual adsorption stage lasts until about 15 min. Then the diffusion starts to slow down due to the lowered concentration difference between gels and solution. The concentration of FITC-AHL inside the PDB gels (5.1 × 10^{-6} mol L^{-1}) equals that of the surrounding solution when the equilibrium was reached, while the concentration of FITC-AHL inside the PDB-alg-Ca gels (4.3 × 10^{-6} mol L^{-1}) was ≈15% lower than that of the surrounding solution at equilibrium. PDB-alg-Ca exhibited identical tends for FITC-AHL uptakes as PDB hydrogels, while the uptake speed was lower, which is tentatively attributed to the increased overall polymer concentration inside the gel.

To use the potential of the bacteria hydrogel system as a whole cell biosensor, the reporter bacterium *E. coli* pLuxR-GFP, whose sensing mechanism is based on the Type I quorum sensing mechanism of *P. aeruginosa*, was used as a model system. The final DMSO concentration in the gels was

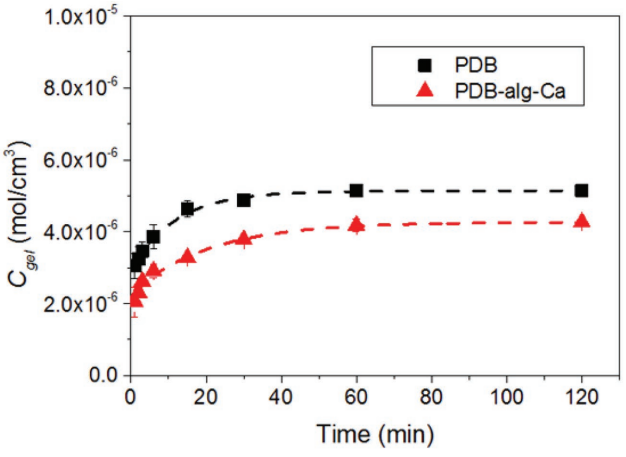

Figure 7. Concentration of FITC-AHL in the PDB hydrogels (3 mg mL^{-1}) and PDB-alg-Ca hydrogels (3 mg mL^{-1} PDB and 5 mg mL^{-1} alginate) over time, as determined by the fluorescence intensity versus concentration standard curve. The data are presented as arithmetic mean ± standard deviation calculated from at least three replicates.

calculated as ≤2% (v/v), which is lower than the reported minimal inhibitory concentration (7–10%) for *E. coli*.[44,45] To investigate the effect of hydrogels on the viability and proliferation of *E. coli* pLuxR-GFP, the optical densities at 600 nm of *E. coli* pLuxR-GFP in LB medium and in PDB-alg-Ca hydrogels were recorded over time using a microplate reader. The three phases of the resulting growth curve, including lag phase, exponential phase and stationary phase, were thus recorded. As shown in **Figure 8**a, *E. coli* pLuxR-GFP in PDB-alg-Ca hydrogels had the same generation time of 32 ± 7 min as that of bacteria in LB medium (33 ± 5), suggesting that the encapsulation in the PDB-alg-Ca hydrogels had negligible effect on the growth rate of *E. coli* pLuxR-GFP under the utilized test conditions. In addition, *E. coli* pLuxR-GFP incubated in LB medium and in PDB-alg-Ca hydrogels showed similar lag time and reached to within the experimental error identical cell densities in the stationary phase. All those results confirm that the PDB-alg-Ca hydrogels possess no obvious detrimental influence on viability and proliferation of encapsulated *E. coli* pLuxR-GFP.

The effect of $3OC_{12}HSL$ on the GFP expression of the reporter bacterium *E. coli* pLuxR-GFP was first studied via monitoring the fluorescence intensity (due to GFP fluorescence) in LB medium and in bulk PDB-alg-Ca hydrogels over time (Figure 8b). Since *E. coli* does not encode enzymes for the production of autoinducers recognized in the LuxR family,[46] false positive signals due to quorum sensing of *E. coli* itself can be neglected. Green fluorescence indicated the level of LuxR induction, which has been shown to correlate closely with the extracellular concentration of the autoinducer $3OC_{12}HSL$.[31] In the presence of 1.0 × 10^{-6} mol L^{-1} $3OC_{12}HSL$, a sharp increase in fluorescence intensity was observed for bacteria in both LB medium and PDB-alg-Ca hydrogels, compared to the faint background increase that was observed for bacteria that were not exposed to $3OC_{12}HSL$ (Figure 8b). The increase of the fluorescence intensity reached a maximum after ≈4–6 h incubation in both LB medium and in PDB-alg-Ca hydrogels, as is indicated by the arrow in Figure 8b. When exposed to $3OC_{12}HSL$, the fluorescence intensity was 13 ± 3 times higher for bacteria in LB medium than without induction. For bacteria in the PDB-alg-Ca hydrogels, the fluorescence intensity was 12 ± 3 times higher than in the absence of autoinducers. The influence of $3OC_{12}HSL$ concentration on the GFP expression of bacteria was studied by monitoring the fluorescence intensity and OD_{600} of *E. coli* pLuxR-GFP in LB medium and bulk PDB-alg-Ca hydrogels (Figure 8c). The fluorescence intensity, normalized to the cell density (fluorescence intensity divided by OD_{600}) and further divided by that observed in the control culture (without exposition to $3OC_{12}HSL$), was used as a relative measure for GFP expression. In the presence of 1 × 10^{-6} to 1 × 10^{-8} mol L^{-1} $3OC_{12}HSL$, the normalized fluorescence intensity was ≈12 times higher than in the absence of autoinducers, which is identical to the results of bacteria entrapped in PDB gels.[32] For bacteria in both LB medium and in the bulk hydrogels, no significant difference in relative GFP expression was observed for all the $3OC_{12}HSL$ concentrations tested. For the following experiments with biosensor arrays, 1 × 10^{-6} mol L^{-1} $3OC_{12}HSL$ was used.

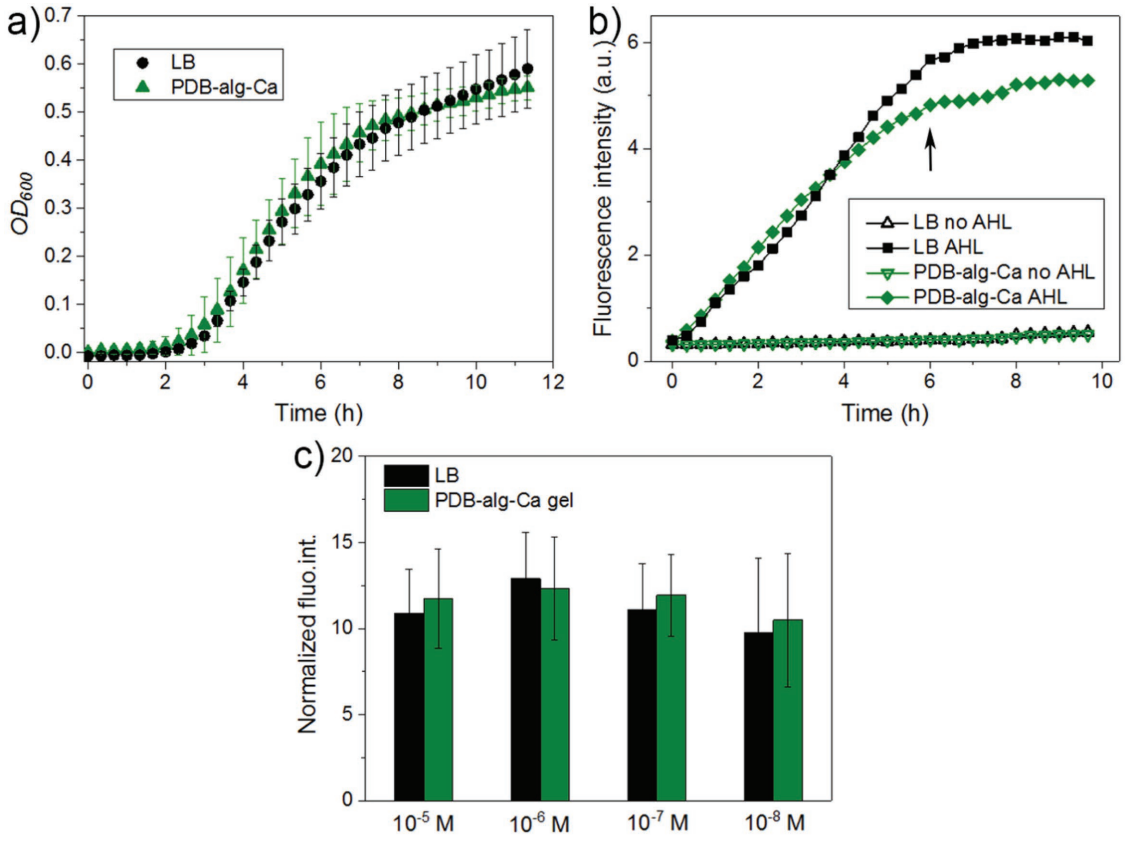

Figure 8. a) OD_{600} growth curves of *E. coli* pLuxR-GFP in LB medium and in bulk PDB-alg-Ca hydrogels, error bars indicate the corresponding standard deviations ($n > 3$); b) fluorescence intensity of *E. coli* pLuxR-GFP in LB medium and in bulk PDB-alg-Ca hydrogels over time with and without autoinducer $3OC_{12}HSL$ (1.0×10^{-6} mol L^{-1}); c) normalized fluorescence intensity per OD_{600} of *E. coli* pLuxR-GFP in LB medium and PDB-alg-Ca gel in the presence of 1×10^{-5}, 1×10^{-6}, 1×10^{-7}, 1×10^{-8} mol L^{-1} $3OC_{12}HSL$ after 6 h incubation (normalized to the fluorescence intensity per OD_{600} in the absence of $3OC_{12}HSL$). The data are presented as arithmetic mean ± standard deviation calculated from three biological replicates, no statistically significant differences calculated from a one-way ANOVA test.

After demonstrating that the reporter bacteria preserved their autoinducer sensing functionality upon encapsulation inside the new mechanically more robust PDB-alg-Ca hybrid hydrogels, biosensor arrays with physically isolated wells were fabricated using a micropatterning method. A commercially available pyramidal microwell array chip was used as template for patterning hydrogels. As shown in **Figure 9**a, the PDMS replica consisted of tightly packed square-pyramid features with 402 ± 7 µm width and 255 ± 6 µm height. The PEGDA microwell system formed by micromolding from this PDMS replica was hence composed of square-pyramidal wells with 409 ± 9 µm width and 229 ± 4 µm height (Figure 9b). The PDB-alg-Ca

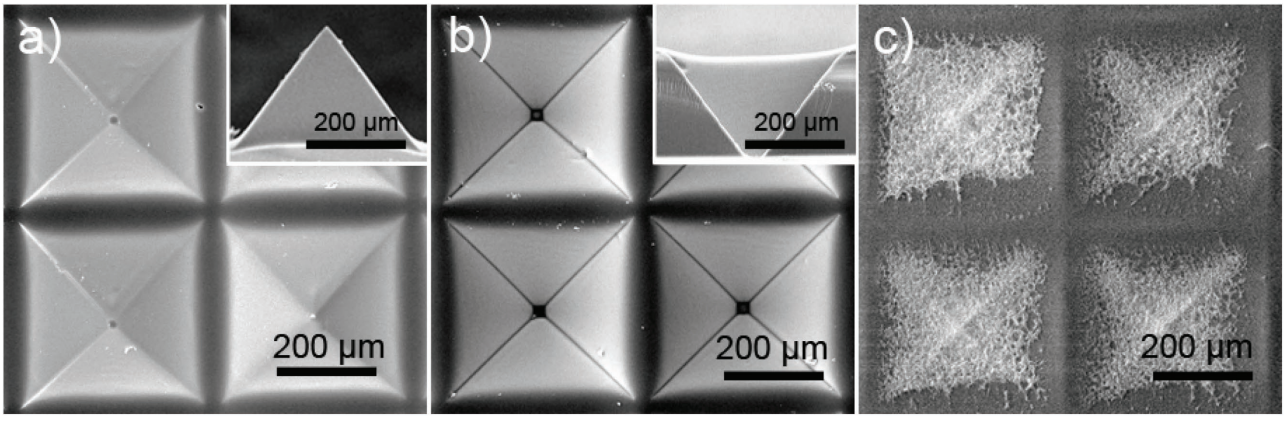

Figure 9. SEM images of a) PDMS mold, insert shows a cross-section image; b) PEGDA microwell arrays, insert shows a cross-section image; c) PDB-alg-Ca micropatterned gels (3 mg mL^{-1} PDB and 5 mg mL^{-1} alginate).

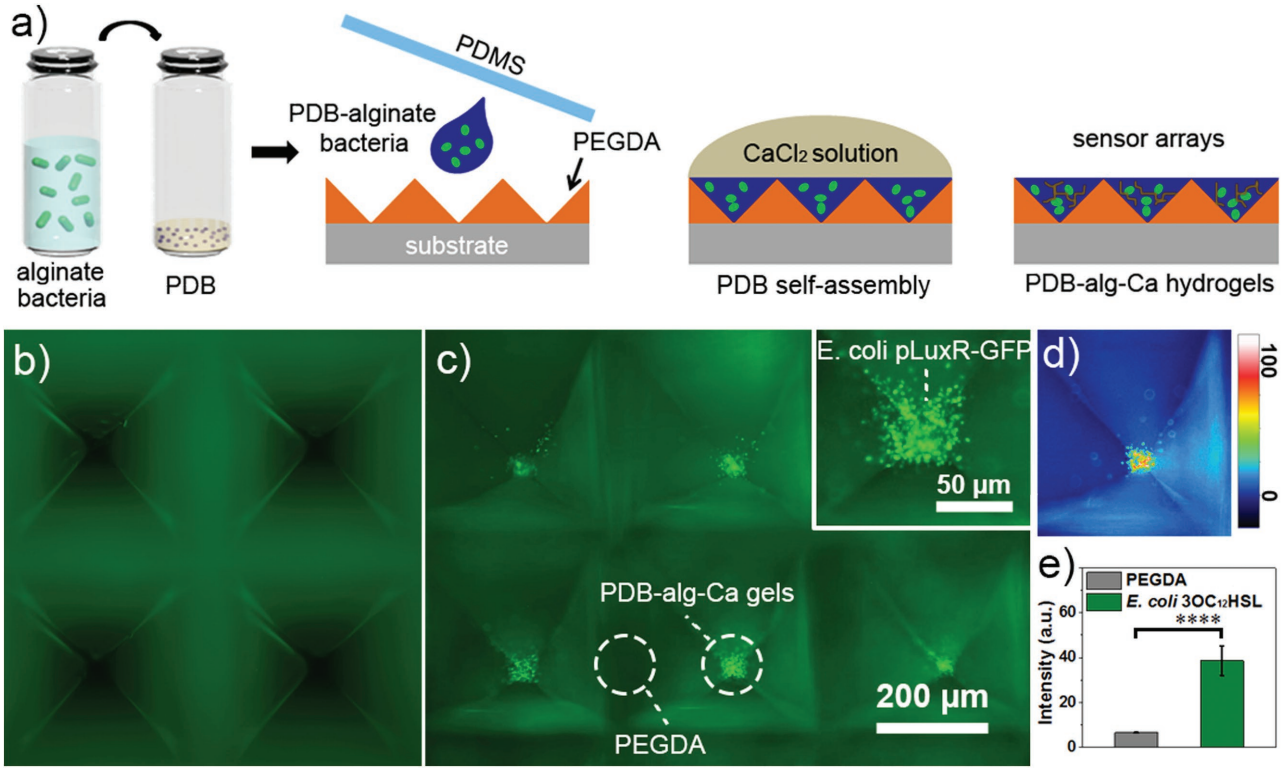

Figure 10. a) Schematic diagram for the fabrication of sensor arrays; fluorescence microscopy images of PDB-alg-Ca hydrogels with *E. coli* pLuxR-GFP encapsulated b) in the absence of and c) in the presence of 1.0×10^{-6} mol L^{-1} $3OC_{12}HSL$, insert is a zoom image of a single microwell; d) heatmap of a single microwell; e) the average intensities of the PEGDA area and PDB-alg-Ca hydrogels area were measured using ImageJ, the error bars indicate the corresponding standard deviations ($n > 15$), $^{****}p < 0.0001$ by a one-way ANOVA test.

hydrogels formed in this template exhibited 392 ± 14 μm width after detachment from the PEGDA microwell arrays and drying (Figure 9c). The decrease in width and height may be caused by the collapse of hydrogel networks during drying process.

The equilibrium swelling ratios of PDB-alg-Ca with different PDB and alginate concentrations in solutions were determined, as shown in Figure S6 (Supporting Information). The swelling ratio of PDB-alg-Ca hydrogels with 4 mg mL^{-1} PDB and 5 mg mL^{-1} alginate was 1.6 ± 0.8%. When the alginate concentration was increased from 5 to 10 mg mL^{-1}, the swelling ratio increased around 5 times. Thus, in the following, PDB-alg-Ca hydrogels with 3 and 5 mg mL^{-1} alginate were used for hydrogel patterning because of the relative low swelling ratio (1.4 ± 0.5%) and high elastic modulus (≈2.5×10^4 Pa).

PDB-alg-Ca hydrogels with encapsulated *E. coli* pLuxR-GFP were patterned using the same template since the sloping sidewalls may help to guide the sedimentation of bacteria and thus intensify the fluorescence signal at the tip of the pyramid. Thus it is possible to minimize the number of bacteria per well for high signal to noise ratio detection. The fabrication process is shown in **Figure 10**a. For easier handling, the PDB-alg-Ca gels were not separated from the PEGDA template. In order to label PEGDA microwell arrays, the fluorescent dye nile red was mixed with PEGDA. Due to the long pass emission filter used in the microscope, the microwell arrays exhibited green color in fluorescence microscopy images. As expected, a small volume of PDB-alg-Ca hydrogels precursor (≈0.02 nL per well) with encapsulated *E. coli* pLuxR-GFP tended to accumulate and set at the bottom of the PEGDA microwell arrays, i.e., at the pyramid tip (Figure 10b,c). When exposed to 1.0×10^{-6} mol L^{-1} $3OC_{12}HSL$, the fluorescence intensity increased markedly due to the GFP expression by the encapsulated *E. coli* pLuxR-GFP. The average of the fluorescence intensity of PDB-alg-Ca hydrogel areas was around 6 times higher than that of PEGDA gel area, as is shown Figure 10e.

When the well was completely filled with PDB-alg-Ca hydrogel, the number of bacteria per well was estimated by multiplying the volume of the well with the number of bacteria per volume determined from the calibrated OD_{600} values. From the curve of the OD_{600}-colony forming units (CFU) shown in Figure S8 (Supporting Information), the bacteria number per volume was estimated as 2.5×10^9 CFU mL^{-1} for an OD_{600} value about 0.5. The well volume was calculated from the measured width of 392 ± 14 μm and height of 229 ± 4 μm. The estimated bacteria numbers per well were $(2.9 \pm 0.3) \times 10^4$. This large number of bacteria per well could average out any possible variance caused by single bacteria.[32,47]

E. coli pLuxR-GFP inside gels tend to form clusters, presumable due to limited movement and confined segregation of dividing cells in the hydrogel network,[48] as shown **Figure 11**a,d. In the absence of $3OC_{12}HSL$, the average fluorescence intensity of the hydrogel array was similar to the background intensity. For instance in Figure 11b the average fluorescence intensity of the hydrogel array element was the

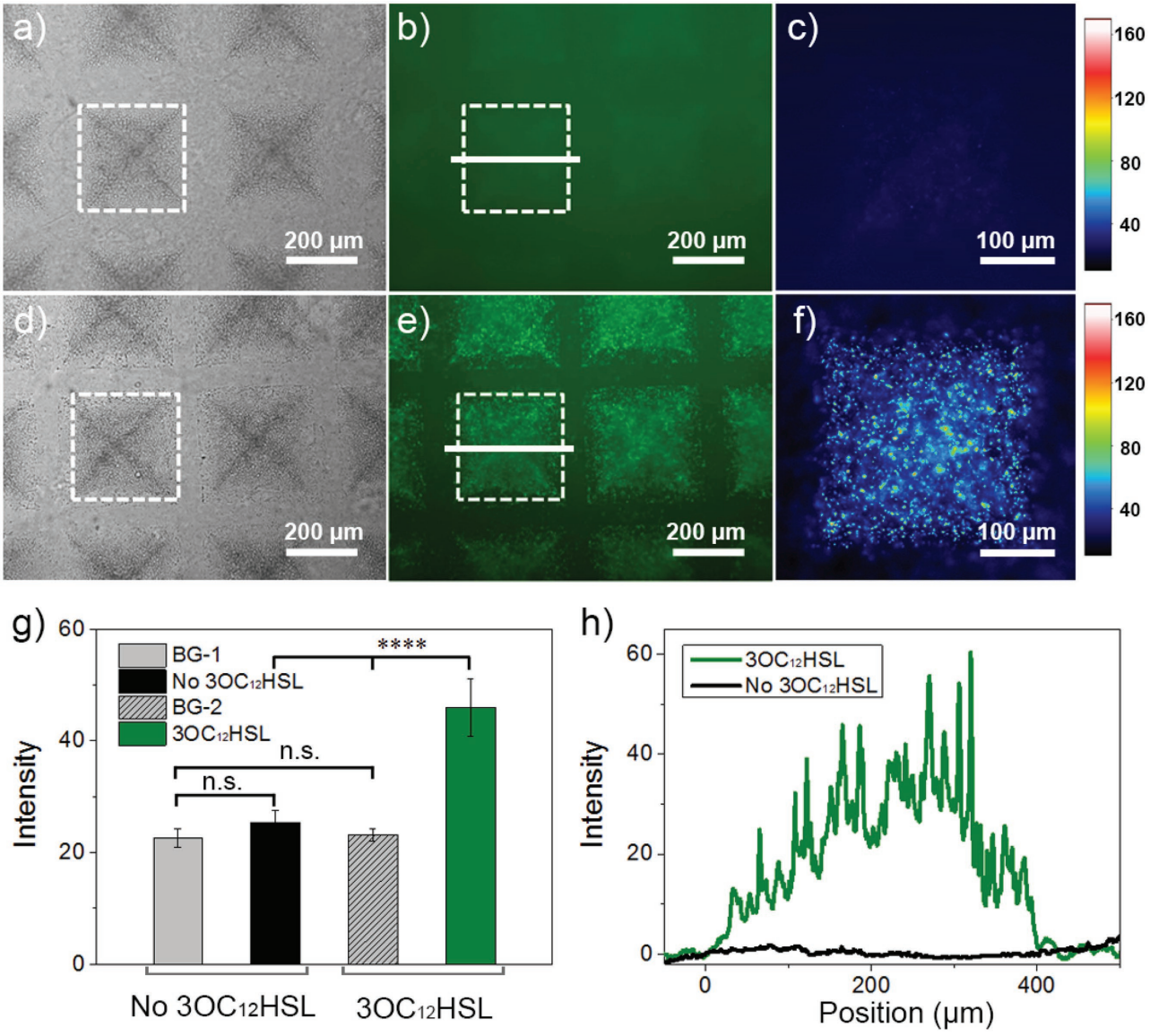

Figure 11. Patterned PDB-alg-Ca hydrogels with *E. coli* pLuxR-GFP in the absence of $3OC_{12}HSL$ after 2 h culture: a) brightfield optical microscopy image, b) fluorescence microscopy image, and c) heatmap of a single well. Patterned PDB-alg-Ca hydrogels with *E. coli* pLuxR-GFP in the presence of 1.0×10^{-6} mol L^{-1} $3OC_{12}HSL$ after 2 h culture: d) brightfield image and e) fluorescence microscopy image; f) heatmap of a single well; g) the average intensity of single wells measured from ImageJ ($n > 40$), ns (not significant) and ****$p < 0.0001$ calculated by a one-way ANOVA test; h) cross-sectional fluorescence intensity plots (corresponding to the white lines shown in (b) and (e). For heatmaps, the false color scale denotes fluorescence intensity indicative of cell densities.

23.1 ± 1.1 relative fluorescence units (RFU), while the background intensity was 22.6 ± 1.7 RFU. When the array was exposed to 1.0×10^{-6} mol L^{-1} $3OC_{12}HSL$, the average fluorescence intensity of the hydrogel array element and the background increased to 46.0 ± 5.1 and 25.4 ± 2.2 RFU, respectively (Figure 11e). The intensity of each well was around 2 times higher after incubation with $3OC_{12}HSL$ than that of the background. Because of the large pattern area, the fluorescence intensity per well was high and the intensity deviations among different wells were relatively low (Figure 11g). As Figure 11f,h demonstrates, the fluorescence intensity of the well middle area is around 25% higher than that of the edge, which is due to the square-pyramid morphology and the mentioned focusing effect. Furthermore, if the hydrogel is released from the PEGDA template, free-standing PDB-alg-Ca hydrogels were obtained. These gel slabs with encapsulated reporter bacteria sense autoinducers in solution, as is shown in Figure S9 (Supporting Information).

Overall, the AHL concentrations tested here are in the range of the reported extracellular concentration of $3OC_{12}HSL$ (1.0×10^{-6} to 1.0×10^{-7} mol L^{-1}) that have been determined close to the site of *P. aeruginosa* infections.[31,49,50] This implies that the PDB-alg-Ca hydrogels with encapsulated reporter bacteria *E. coli* pLuxR-GFP may serve as sensing devices that is sensitive enough to detect the $3OC_{12}HSL$ natively produced by *P. aeruginosa* biofilms.

4. Conclusions

In summary, reinforced supramolecular hydrogels that are formed by the combined supramolecular self-assembly approaches and ionic crosslinking afford a simple and effective method to encapsulate autoinducer-reporting bacteria in microwell and microparticle formats. The two assembly mechanisms do not interfere with each other and despite the more than fourfold increased elastic modulus of hydrogels dye-labelled autoinducers were only marginally hindering in diffusion into the hybrid hydrogel compared to neat PDB hydrogels. By using PEGDA templates, reporter bacteria-loaded hydrogels with controllable shape and size defined by the template were obtained. Inside these PDB-alg-Ca hydrogels, *E. coli* pLuxR-GFP was observed to proliferate with generation time of 32 ± 7 min, which is comparable to conventional LB medium. Upon exposure to 1.0×10^{-6} mol L^{-1} $3OC_{12}HSL$, the embedded bacteria in bulk gels exhibited 12 ± 3 times increase in fluorescence intensity due to GFP expression as a response to the autoinducers. This approach was finally shown to be compatible with micropatterning strategies to afford autoinducer-reporting PDB-alg-Ca hydrogels that are useful for the detection of *N*-acyl homoserine lactone autoinducers of *P. aeruginosa*. This approach can be expanded as a generic platform to other reporter bacteria and autoinducers as a potentially generally applicable strategy to sensitively detect different bacteria via their secreted autoinducers at relevant concentrations.

Supporting Information

Supporting Information is available from the Wiley Online Library or from the author.

Acknowledgements

The authors thank Dipl-Ing. Gregor Schulte for technical support and Dr. Yvonne Voss for helping with the initial experiments. The authors would like to acknowledge funding received for the project from the funding program of the Federal Ministry of Economics and Technology in Germany, "Central Innovation Programme SME" (ZIM, KF2589507SK4), that is carried out together with our cooperation partner Quh-Lab (Siegen), financial support from the EU (ERC project ASMIDIAS, Grant no. 279202), and the University of Siegen.

Conflict of Interest

The authors declare no conflict of interest.

Keywords

alginate, bioencapsulation, biosensor, micropatterning, quorum sensing, supramolecular hydrogel

Received: May 21, 2017
Revised: June 27, 2017
Published online:

[1] N. T. Thet, W. D. Jamieson, M. Laabei, J. D. Mercer-Chalmers, A. T. A. Jenkins, *J. Phys. Chem. B* **2014**, *118*, 5418.
[2] S. Haas, N. Hain, M. Raoufi, S. Handschuh-Wang, T. Wang, X. Jiang, H. Schönherr, *Biomacromolecules* **2015**, *16*, 832.
[3] M.-M. Sadat Ebrahimi, Y. Voss, H. Schönherr, *ACS Appl. Mater. Interfaces* **2015**, *7*, 20190.
[4] A. Beyer, S. Pollok, A. Rudloff, D. Cialla-May, K. Weber, J. Popp, *Macromol. Biosci.* **2016**, *16*, 1325.
[5] K.-S. Tücking, V. Grützner, R. E. Unger, H. Schönherr, *Macromol. Rapid Commun.* **2015**, *36*, 1248.
[6] S. Malic, K. E. Hill, A. Hayes, S. L. Percival, D. W. Thomas, D. W. Williams, *Microbiology* **2009**, *155*, 2603.
[7] N. T. Thet, A. T. A. Jenkins, *Electrochem. Commun.* **2015**, *59*, 104.
[8] F. Paladini, M. Pollini, A. Sannino, L. Ambrosio, Progress and Perspectives in the Management of Wound Infections. In *Wound Healing - New insights into Ancient Challenges*, (Ed.: V. A. Alexandrescu), InTech, Rijeka, **2016**, Chapter 20, pp. 435–456.
[9] N. T. Thet, D. R. Alves, J. E. Bean, S. Booth, J. Nzakizwanayo, A. E. R. Young, B. V. Jones, A. T. A. Jenkins, *ACS Appl. Mater. Interfaces* **2016**, *8*, 14909.
[10] S. L. Percival, K. E. Hill, D. W. Williams, S. J. Hooper, D. W. Thomas, J. W. Costerton, *Wound Repair Regen.* **2012**, *20*, 647.
[11] L. A. Hawver, S. A. Jung, W. L. Ng, *FEMS Microbiol. Rev.* **2016**, *40*, 738.
[12] K. Papenfort, B. L. Bassler, *Nat. Rev. Microbiol.* **2016**, *14*, 576.
[13] M. S. Blackledge, R. J. Worthington, C. Melander, *Curr. Opin. Pharmacol.* **2013**, *13*, 699.
[14] A. Gupta, J. L. Terrell, R. Fernandes, M. B. Dowling, G. F. Payne, S. R. Raghavan, W. E. Bentley, *Biotechnol. Bioeng.* **2013**, *110*, 552.
[15] T. Karlsson, M. V. Turkina, O. Yakymenko, K.-E. Magnusson, E. Vikström, A. Hauser, *PLoS Pathogens* **2012**, *8*, e1002953.
[16] M. Park, S.-L. Tsai, W. Chen, *Sensors* **2013**, *13*, 5777.
[17] Š. Selimović, J. Oh, H. Bae, M. Dokmeci, A. Khademhosseini, *Polymers* **2012**, *4*, 1554.
[18] J. L. Drury, D. J. Mooney, *Biomaterials* **2003**, *24*, 4337.
[19] L. Gasperini, J. F. Mano, R. L. Reis, *J. R. Soc. Interface* **2014**, *11*, 20140817.
[20] S. Rokka, P. Rantamäki, *Eur. Food Res. Technol.* **2010**, *231*, 1.
[21] D. M. Headen, G. Aubry, H. Lu, A. J. Garcia, *Adv. Mater.* **2014**, *26*, 3003.
[22] A. Khavari, M. Nydén, D. A. Weitz, A. J. Ehrlicher, *Sci. Rep.* **2016**, *6*, 30854.
[23] M. Chau, M. Abolhasani, H. Therien-Aubin, Y. Li, Y. Wang, D. Velasco, E. Tumarkin, A. Ramachandran, E. Kumacheva, *Biomacromolecules* **2014**, *15*, 2419.
[24] L. Gasperini, J. F. Mano, R. L. Reis, *J. R. Soc. Interface* **2014**, *11*, 20140817.
[25] S. Rathore, P. M. Desai, C. V. Liew, L. W. Chan, P. W. S. Heng, *J. Food Eng.* **2013**, *116*, 369.
[26] S-G. Zhang, *Nat. Mater.* **2004**, *3*, 7.
[27] X. Du, J. Zhou, J. Shi, B. Xu, *Chem. Rev.* **2015**, *115*, 13165.
[28] K. J. van Bommel, C. van der Pol, I. Muizebelt, A. Friggeri, A. Heeres, A. Meetsma, B. L. Feringa, J. van Esch, *Angew. Chem., Int. Ed.* **2004**, *43*, 1663.
[29] J. Zhou, J. Li, X. Du, B. Xu, *Biomaterials* **2017**, *129*, 1.
[30] X-Q. Dou, C-L. Feng, *Adv. Mater.* **2017**, *29*, 1604062.
[31] N. Saeidi, C. K. Wong, T. M. Lo, H. X. Nguyen, H. Ling, S. S. Leong, C. L. Poh, M. W. Chang, *Mol. Syst. Biol.* **2011**, *7*, 521.
[32] P. Li, X. Q. Dou, C. L. Feng, M. Müller, M-W. Chang, M. Frettlöh, H. Schönherr, *Langmuir* **2017**, in press, http://dx.doi.org/10.1021/acs.langmuir.7b00749.
[33] P. Li, X. Q. Dou, C. L. Feng, D. Zhang, *Soft Matter* **2013**, *9*, 3750.

[34] G. F. Liu, D. Zhang, C. L. Feng, *Angew. Chem., Int. Ed.* **2014**, *53*, 7789.
[35] K. Y. Lee, D. J. Mooney, *Prog. Polym. Sci.* **2012**, *37*, 106.
[36] H. Hosseinkhani, M. Hosseinkhani, F. R. Tian, H. Kobayashi, Y. Tabata, *Tissue Eng.* **2007**, *13*, 11.
[37] P. Li, X.-Q. Dou, Y-T. Tang, S. Zhu, J. Gu, C.-L. Feng, D. Zhang, *J. Colloid Interface Sci.* **2012**, *387*, 115.
[38] X.-Q. Dou, P. Li, D. Zhang, C.-L. Feng, *Soft Matter* **2012**, *8*, 3231.
[39] C. Sartori, D. S. Finch, B. Ralph, K. Gilding, *Polymer* **1997**, *38*, 43.
[40] W. Edwards, D. K. Smith, *J. Am. Chem. Soc.* **2014**, *136*, 1116.
[41] A. R. Hirst, D. K. Smith, M. C. Feiters, H. P. M. Geurts, *Chem. Eur. J.* **2004**, *10*, 5901.
[42] K. Akamatsu, K. Maruyama, W. Chen, A. Nakao, S.-I. Nakao, *J. Colloid Interface Sci.* **2011**, *363*, 707.
[43] S. Sathaye, A. Mbi, C. Sonmez, Y. Chen, D. L. Blair, J. P. Schneider, D. J. Pochan, *WIRES: Nanomed. Nanobiotechnol.* **2015**, *7*, 34.
[44] H. Basch, H. H. Gadebusch, *Appl. Microbiol.* **1968**, *16*, 1953.
[45] S. Negin, M. R. Gokel, M. B. Patel, S. L. Sedinkin, D. C. Osborn, G. W. Gokel, *RSC Adv.* **2015**, *5*, 8088.
[46] B. M. M. Ahmer, *Mol. Microbiol.* **2004**, *52*, 933.
[47] R. H. Hansen, A. C. Timm, C. M. Timm, A. N. Bible, J. L. Morrell-Falvey, D. A. Pelletier, M. L. Simpson, M. J. Doktycz, S. T. Retterer, *PLoS ONE* **2016**, *11*, e0155080.
[48] J. Z. Crouse, K. M. Mahuta, B. A. Mikulski, J. N. Harvestine, X. Guo, J. C. Lee, M. G. Kaltchev, K. S. Midelfort, C. S. Tritt, J. Chen, *J. Appl. Biomater. Funct. Mater.* **2015**, *13*, e326.
[49] J. P. Pearson, L. Passador, B. H. Iglewski, E. P. Greenberg, *Proc. Natl. Acad. Sci. USA* **1995**, *92*, 1490.
[50] T. S. Charlton, R. De Nys, A. Netting, N. Kumar, M. Hentzer, M. Givskov, S. Kjelleberg, *Environ. Microbiol.* **2000**, *2*, 530.

